Pion Transverse Momentum Spectrum, Elliptic Flow and Interferometry in the Granular Source Model in Ultra-Relativistic Heavy Ion Collisions

Jing Yang[1], Yan-Yu Ren[2] and Wei-Ning Zhang[1,2]

[1]School of Physics and Optoelectronic Technology,
Dalian University of Technology, Dalian, China
[2]Department of Physics, Harbin Institute of Technology, Harbin, China

Abstract

We systematically investigate the pion transverse momentum spectrum, elliptic flow, and Hanbury-Brown-Twiss (HBT) interferometry in the granular source model of quark-gluon plasma droplets in ultra-relativistic heavy ion collisions. The granular source model can well reproduce the experimental results of the Au-Au collisions at $\sqrt{s_{NN}} = 200$ GeV and the Pb-Pb collisions at $\sqrt{s_{NN}} = 2.76$ TeV with different centralities. We examine the parameters of the granular source models with an uniform and Woods-Saxon initial energy distributions in a droplet. The parameters exhibit certain regularities for collision centrality and energy.

1 Introduction

Single particle transverse momentum spectrum, elliptic flow, and Hanbury-Brown-Twiss (HBT) interferometry are three important final particle observables in high energy heavy ion collisions. They reflect the characters of the particle-emitting sources in different aspects and at different stages. Therefore, a combined investigation of these observables can provide very strong constrains for source models.

So far, much progress has been made in understanding the experimental data of the heavy ion collisions at the top energies of the Relativistic Heavy Ion Collider (RHIC) [1, 2, 3, 4, 5, 6, 7, 8, 9]. However, more detailed investigations of the physics beneath the data through multiobservable analyses are still needed. On the other hand, the experimental data of the Pb-Pb collisions at $\sqrt{s_{NN}} = 2.76$ TeV at the Large Hadron Collider (LHC) have been recently published [10, 11, 12, 13]. It is an ambitious goal for models to explain the experimental data of particle spectra, elliptic flow, and HBT interferometry in different centrality region consistently for the heavy ion collisions at the RHIC and LHC.

In Refs. [14, 15, 16], W. N. Zhang *et al.* proposed and developed a granular source model of quark-gluon plasma (QGP) droplets to explain the HBT data of the RHIC experiments [17, 18, 19, 20]. In Ref. [21, 22], the granular source model was used to explain the pion transverse momentum spectrum and HBT data of the most central heavy ion collisions at the RHIC and LHC. Motivated by these successes, we systematically investigate the pion transverse momentum spectrum, elliptic flow, and HBT interferometry for the granular sources in the heavy ion collisions at the RHIC and LHC energies with different centralities. The granular source parameters for an uniform and Woods-Saxon initial energy distributions in a droplet are examined and compared.

2 Granular Source Model

The granular source model of QGP droplets regards the whole source evolution as the superposition of the evolutions of many QGP droplets. Each droplet has a position-dependent initial velocity and evolves hydrodynamically. The model construction is based on the following suggestions. In the heavy ion collisions at top RHIC energies and LHC energies, the created strong coupled QGP (sQGP) systems at central rapidity region may reach local equilibrium at a very short time, and then expand rapidly along the beam direction (z-axis). Because the local equilibrium system is not uniform in the transverse plane (x-y plane) [23]. The system may form many tubes along the beam direction during the subsequent fast longitudinal expansion and finally fragment into many QGP droplets with the effects of "sausage" instability, surface tension, and bulk viscosity [15, 24, 25, 26].

As in Ref. [15], we suppose the QGP droplets of the granular source initially distribute within a cylinder along z-axis by

$$\frac{dN_d}{dx_0 dy_0 dz_0} \propto \left[1 - e^{-(x_0^2+y_0^2)/\Delta\mathcal{R}_T^2}\right]\theta(\mathcal{R}_T - \rho_0) \times\theta(\mathcal{R}_z - |z_0|). \quad (1)$$

Here $\rho_0 = \sqrt{x_0^2 + y_0^2}$ and z_0 are the initial transverse and longitudinal coordinates of the droplet centers. The parameters $\mathcal{R}_T$ and $\mathcal{R}_z$ describe the initial transverse and longitudinal sizes of the source, and $\Delta\mathcal{R}_T$ is a transverse shell parameter [15].

In Ref. [22], the Bjorken hypothesis [27] of longitudinal boost-invariant is used to describe the longitudinal velocity of droplet for the most central collisions, and the transverse velocity of droplet has a form of exponential power. Considering the longitudinal velocity of droplet varying with collision centrality, we introduce here also a longitudinal power parameter, which will be determined by experimental data, to describe the longitudinal velocity phenomenologically. The initial velocities

of the droplets in granular source frame are assumed as [15]

$$v_{\mathrm{d}i} = \mathrm{sign}(r_{0i}) \cdot a_i \left(\frac{|r_{0i}|}{\mathcal{R}_i} \right)^{b_i}, \qquad i = 1,\, 2,\, 3, \tag{2}$$

where r_{0i} is x_0, y_0, or z_0 for $i = 1$, 2, or 3, and sign(r_{0i}) denotes the signal of r_{0i}, which ensures an outward droplet velocity. In Eq. (2), $\mathcal{R}_i = (\mathcal{R}_T, \mathcal{R}_T, \mathcal{R}_z)$, $a_i = (a_x, a_y, a_z)$ and $b_i = (b_x, b_y, b_z)$ are the magnitude and exponent parameters in x, y, and z directions, which are associated with the early thermalization and pressure gradients of the system at the breakup time. It is also convenient to use the equivalent parameters $\overline{a}_T = (a_x + a_y)/2$ and $\Delta a_T = a_x - a_y$ instead of a_x and a_y. The parameters $\overline{a}_T$ and Δa_T describe the transverse expansion and asymmetric dynamical behavior of the system at the breakup time, respectively. For simplicity, we take $b_x = b_y = b_T$ in calculations. The parameters b_T and b_z describe the coordinate dependence of exponential power in transverse and longitudinal directions.

In the calculations of the hydrodynamical evolution of the droplet, we use the equation of state (EOS) of the S95p-PCE165-v0 [28], which combines the lattice QCD data at high temperature with the hadron resonance gas at low temperature. We assume systems fragment when reaching a certain local energy density ϵ_0, and take the initial energy density of the droplets to be 2.2 GeV/fm^3 for all considered collisions for simplicity [22]. The initial droplet radius r_0 is supposed satisfying a Gaussian distribution with the standard deviation $\sigma_d = 2.5$ fm in the droplet local frame [22]. We consider an uniform initial energy distribution in droplet and a Woods-Saxon distribution,

$$\epsilon(r) = \epsilon_0 \frac{1}{e^{\frac{r-r_0}{a}} + 1}, \tag{3}$$

where $a = 0.1 r_0$.

With the evolution of the hot droplets, the final pions freeze out at temperature T_f with the momenta obeying Bose-Einstein distribution. To include the resonance decayed pions emitted later as well as the directly produced pions at chemical freeze out earlier, a wide region of T_f is considered with the probability [22]

$$\begin{aligned} \frac{dP}{dT_f} \quad \propto \quad & f_{\mathsf{dir}}\, e^{-\frac{T_{\mathsf{chem}} - T_f}{\Delta T_{\mathsf{dir}}}} + (1 - f_{\mathsf{dir}}) \\ & \times e^{-\frac{T_{\mathsf{chem}} - T_f}{\Delta T_{\mathsf{dec}}}}, \quad (T_{\mathsf{chem}} > T_f > 80 \text{ MeV}), \end{aligned} \tag{4}$$

where f_{dir} is the fraction of the direct emission around the chemical freeze out temperature T_{chem}, ΔT_{dir} and ΔT_{dec} are the temperature widths for the direct and decay emissions, respectively. In the calculations, we take $f_{\mathsf{dir}} = 0.75$, $\Delta T_{\mathsf{dir}} = 10$ MeV, and $\Delta T_{\mathsf{dec}} = 90$ MeV as in Ref. [22]. The value of T_{chem} is taken to be 165 MeV as it be taken in the S95p-PCE165-v0 EOS [28].

After fixing the parameters used in the calculations of hydrodynamical evolution and freeze-out temperature, the free model parameters are the three source geometry parameters (R_T, ΔR_T, R_z) and the five droplet velocity parameters ($\overline{a}_T$, Δa_T, a_z, b_T, b_z). They are associated with the initial sizes, expansion, and directional asymmetry of system, and have significant influence on the observables of pion momentum sprectra, elliptic flow, and HBT radii in the granular source model. In next section, we will determine these parameters by the experimental data of these observable, and examine their variations with collision energy and centrality for the heavy ion collisions at the RHIC and LHC.

3 Results of Pion Momentum Spectrum, Elliptic Flow and Interferometry

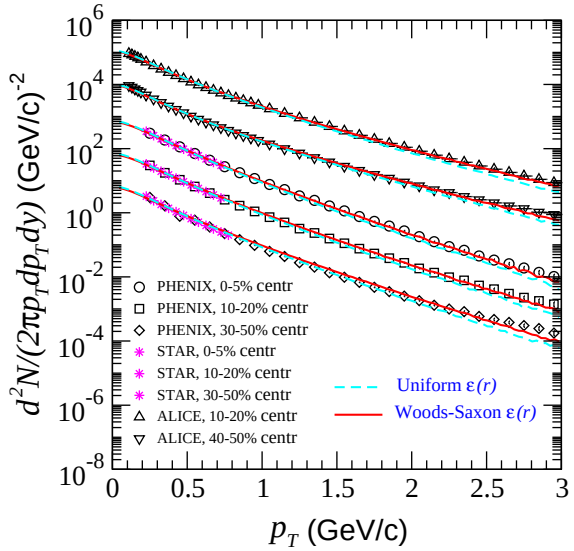

Figure 1: (Color online) The pion transverse momentum spectra of the granular sources for the RHIC Au-Au collisions at $\sqrt{s_{NN}} = 200$ GeV and the LHC Pb-Pb collisions at $\sqrt{s_{NN}} = 2.76$ TeV, for the uniform and Woods-Saxon initial energy distributions in a droplet. The experimental data of PHENIX [31], STAR [32], and ALICE [10] are also plotted.

In high energy heavy ion collisions, the invariant momentum distribution of final particles can be written in the form of a Fourier series [29, 30],

$$E\frac{d^3N}{d^3p} = \frac{1}{2\pi}\frac{d^2N}{p_T dp_T dy}\left[1 + \sum_n 2v_n \cos(n\phi)\right], \tag{5}$$

where E is the energy of the particle, p_T is the transverse momentum, y is the rapidity, and ϕ is the azimuthal angle with respect to the reaction plane. In Eq. (5), the first term on right is the transverse momentum spectrum in the rapidity region dy, and the second harmonic coefficient v_2 in the summation is called elliptic flow.

In Fig. 1, we plot the pion transverse momentum spectra of the granular sources with the uniform and Woods-Saxon initial energy distributions in a droplet. The experimental data of the Au-Au collisions at $\sqrt{s_{NN}} = 200$ GeV at the RHIC [31, 32] and the Pb-Pb collisions at $\sqrt{s_{NN}} = 2.76$ TeV at the LHC [10] are also plotted. In Fig. 2, we plot the pion elliptic flow results of the granular sources with the uniform and Woods-Saxon initial energy distributions, and the experimental data of the Au-Au collisions [33] and the Pb-Pb collisions [11].

The transverse momentum spectrum and elliptic flow of the granular sources are well in agreement with the experimental data, except for the elliptic flow results at

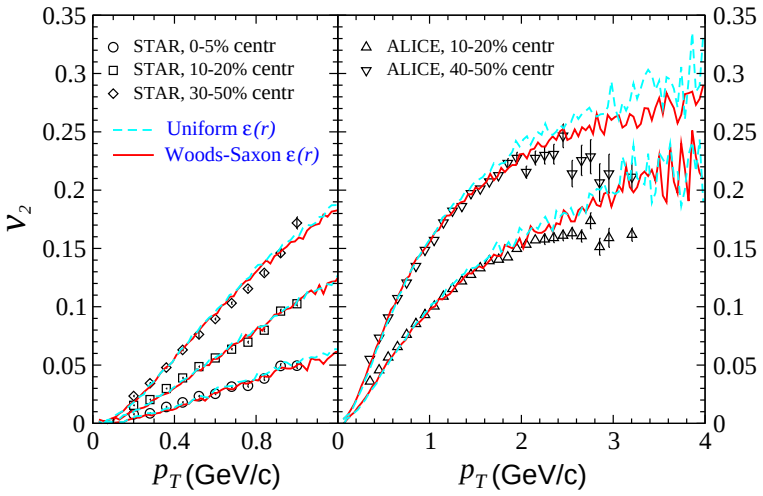

Figure 2: (Color online) The pion elliptic flow of the granular sources for the RHIC Au-Au collisions at $\sqrt{s_{NN}} = 200$ GeV and the LHC Pb-Pb collisions at $\sqrt{s_{NN}} = 2.76$ TeV, for the uniform and Woods-Saxon initial energy distributions in a droplet. The experimental data of STAR [33], and ALICE [11] are also plotted.

$p_T > 2$ GeV/c. The differences between the results of the granular sources with the uniform and Woods-Saxon initial energy distributions are small. The experimental data of the momentum spectrum and elliptic flow at the same centralities can simultaneously give the strong constraints to the velocity parameters of the granular sources. After then, the geometry parameters of the granular sources for the collisions with the different centralities can be further determined by the experimental data of HBT interferometry at the same centralities.

Two-particle HBT correlation function is defined as the ratio of the two-particle momentum spectrum $P(\mathbf{p}_1, \mathbf{p}_2)$ to the product of two single-particle momentum spectra $P(\mathbf{p}_1)P(\mathbf{p}_2)$. It has been widely used to extract the space-time geometry, dynamic and coherence information of the particle-emitting source in high energy heavy ion collisions [34, 35, 36, 37, 38]. In the usual HBT analysis in high energy heavy ion collisions, the two-pion correlation functions are fitted by the Gaussian parameterized formula

$$C(q_{\rm out}, q_{\rm side}, q_{\rm long}) = 1 + \lambda\, e^{-R^2_{\rm out}q^2_{\rm out} - R^2_{\rm side}q^2_{\rm side} - R^2_{\rm long}q^2_{\rm long}}, \qquad (6)$$

where $q_{\rm out}$, $q_{\rm side}$, and $q_{\rm long}$ are the Bertsch-Pratt variables [39, 40], which denote the components of the relative momentum $\mathbf{q} = \mathbf{p}_1 - \mathbf{p}_2$ in transverse out and side directions and in longitudinal direction, respectively. In Eq. (6) λ is chaoticity parameter of source, $R_{\rm out}$, $R_{\rm side}$, and $R_{\rm long}$ are the HBT radii in out, side, and long directions.

We plot in Fig. 3 the two-pion HBT results for the granular sources and the experimental data of the RHIC Au-Au collisions [20] and the LHC Pb-Pb collisions [13] with the same centralities as the experimental data of the spectrum and elliptic

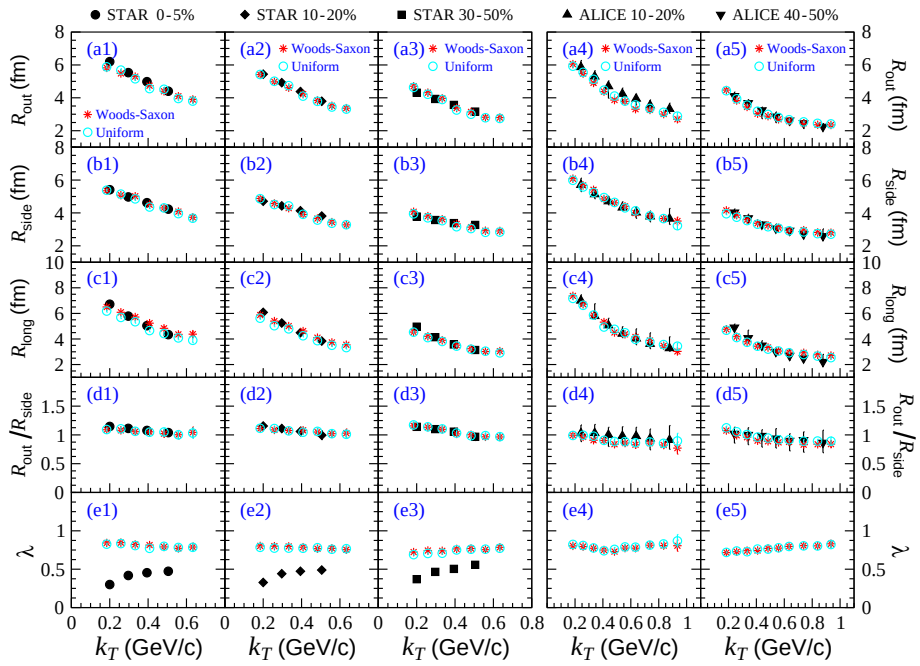

Figure 3: (Color online) The HBT results of the granular sources for the uniform and Woods-Saxon initial energy distribution, and the experimental data for the Au-Au collisions at the RHIC [20] and the Pb-Pb collisions at the LHC [13] with different centralities.

flow. Here, k_T is the transverse momentum of pion pair. One can see that the granular source models can well reproduce the experimental HBT radii and their variations with k_T. The results of the chaotic parameters λ of the granular sources are larger than the experimental data, because there are many effects in experiments can decrease λ [34, 35, 36, 37, 38], which exceed our considerations.

In Table 1, we present the parameters of the granular sources with uniform initial energy distribution in a droplet, determined by the experimental data of the momentum spectra, elliptic flow, and HBT radii. The values of the source geometry parameters indicate that the sources are a short cylinder with small shell effect (small ΔR_T). For certain collision energy, the source geometry parameters R_T, ΔR_T and R_z increase with the collision centralities. However, for the 10-20% centrality, these geometry parameters for the LHC collisions are larger than those for the RHIC collisions. The large difference between the droplet velocity parameters b_T and b_z indicates the different dynamical behaviors of the sources in the transverse and long directions. The parameter Δa_T increases with decreasing centrality. And, the values of $\overline{a}_T$ and a_z are almost independent of collision centrality. A detail analysis on the relationships between the source parameters and the granular source space-time evolution can be seen in Ref. [41].

Table 1: The geometry parameters (in fm unit) and velocity parameters of the granular sources with uniform initial energy distribution in a droplet.

Centrality	$\mathcal{R}_T$	$\Delta\mathcal{R}_T$	$\mathcal{R}_z$	$\overline{a}_T$	Δa_T	a_z	b_T	b_z
RHIC, 0–5 %	5.8	0.7	3.9	0.469	0.066	0.593	0.76	0.13
RHIC, 10–20%	4.5	0.5	2.9	0.454	0.115	0.593	0.56	0.11
RHIC, 30–50%	2.5	0.3	0.5	0.437	0.156	0.593	0.37	0.06
LHC, 10–20%	6.0	0.9	5.5	0.431	0.092	0.592	0.35	0.13
LHC, 40–50%	2.5	0.4	1.8	0.407	0.131	0.590	0.23	0.03

Table 2: The geometry parameters (in fm unit) and velocity parameters of the granular sources with Woods-Saxon initial energy distribution in a droplet.

Centrality	$\mathcal{R}_T$	$\Delta\mathcal{R}_T$	$\mathcal{R}_z$	$\overline{a}_T$	Δa_T	a_z	b_T	b_z
RHIC, 0–5 %	5.8	0.7	5.1	0.469	0.066	0.52	0.76	0.13
RHIC, 10–20%	4.5	0.5	4.0	0.457	0.122	0.52	0.56	0.11
RHIC, 30–50%	2.8	0.3	1.8	0.453	0.156	0.52	0.37	0.06
LHC, 10–20%	6.0	0.9	5.5	0.496	0.092	0.59	0.43	0.13
LHC, 40–50%	2.5	0.4	1.8	0.434	0.127	0.59	0.23	0.03

In Table 2, we present the parameters of the granular sources with Woods-Saxon distribution of initial energy in a droplet, determined by the experimental data of the momentum spectra, elliptic flow, and HBT radii. By Comparing the two set parameters in Table 1 and Table 2, one can see that there are some differences between the R_z and a_z values for the RHIC collisions. Also, for the LHC collisions, the values of $\bar{a}_T$ for for the granular sources with the Woods-Saxon distribution are larger.

4 Summary and Conclusions

We systemically investigate the pion transverse momentum spectrum, elliptic flow, and HBT interferometry in the granular source model for the heavy ion collisions at the RHIC highest energy and the LHC energy. The centrality dependence of the observables at the two energies are examined. By comparing the granular source results with the experimental data of the Au-Au collisions at $\sqrt{s_{NN}} = 200$ GeV at the RHIC and the Pb-Pb collisions at $\sqrt{s_{NN}} = 2.76$ TeV at the LHC with different collision centralities, we investigate the geometry and velocity parameters in the granular source models with an uniform and Woods-Saxon initial energy distributions in a droplet. The parameters as a function of collision centrality and energy are examined. Our investigations indicate that the granular source model can well reproduce the experimental data of pion transverse momentum spectra, elliptic flow, and HBT radii in the Au-Au collisions at $\sqrt{s_{NN}} = 200$ GeV with 0–5%, 10–20%, and 30–50% centralities [20, 31, 32, 33], and in the Pb-Pb collisions at $\sqrt{s_{NN}} = 2.76$ TeV with 10–20% and 40–50% centralities [10, 11, 13]. The experimental data of pion momentum spectra, elliptic flow, and HBT radii impose very strict constraints on the parameters in the granular source model. They exhibit certain regularities for collision centrality and energy.

Acknowledgement

This work was supported by the National Natural Science Foundation of China, Contract No. 11275037.

References

[1] I. Arsene et al. (BRAHMS Collaboration), Nucl. Phys. A **757**, 1 (2005); B. B. Back et al. (PHOBOS Collaboration), *ibid.*, 28; J. Adams et al. (STAR Collaboration), *ibid.*, 102; K. Adcox et al. (PHENIX Collaboration), *ibid.*, 184.

[2] J. Lajoie (PHENIX Collaboration), J. Phys. G **34**, S191 (2007); L. Ruan (STAR Collaboration), *ibid.*, S199; I. G. Bearden (BRAHMS Collaboration), *ibid.*, S207; D. J. Hofman (PHOBOS Collaboration), *ibid.*, S217; M. C. de la Barca (STAR Collaboration), *ibid.*, S225.

[3] J. P. Blaizot, J. Phys. G **34**, S243 (2007); L. McLerran, *ibid.*, S583.

[4] A. Franz (PHENIX Collaboration), J. Phys. G **35**, 104002 (2008); R. Debbe (BRAHMS Collaboration), *ibid.*, 104004; B. Wosiek (PHOBOS Collaboration), *ibid.*, 104005; B. Mohanty (STAR Collaboration), *ibid.*, 104006; T. C. Awes (PHENIX Collaboration), *ibid.*, 104007.

[5] L. McLerran, J. Phys. G **35**, 104001 (2008); R. Venugopalan, *ibid.*, 104003; R. K. Seto, *ibid.*, 104043; E. Shuryak, *ibid.*, 104044.

[6] W. A. Zajc, Nucl. Phys A **830**, 3c (2009).

[7] S. Bathe (PHENIX Collaboration), J. Phys. G **38**, 124001 (2011). H. Masui (STAR Collaboration), *ibid.*, 124002; S. Esumi (PHENIX Collaboration), *ibid.*, 124010; P. Sorensen (STAR Collaboration), *ibid.*, 124029.

[8] B. Schenke, J. Phys. G **38**, 124009 (2011); F. Antinori, *ibid.*, 124038.

[9] U. A. Wiedemann, Nucl. Phys A **904-905**, 3c (2013); B. Hippolyte, D. H. Rischke, *ibid.*, 318c.

[10] B. Abelev *et al.* (ALICE Collaboration), Phys. Rev. C **88**, 044910 (2013).

[11] R. Snellings (ALICE Collaboration), J Phys. G **38**, 124013 (2011).

[12] K. Aamodt *et al.* (ALICE Collaboration), Phys. Lett. B **696**, 328 (2011).

[13] A. Kisiel on behalf of ALICE Collaboration, talk at The Seventh Workshop on Particle Correlations and Femtoscopy, September 20-24, 2011, Tokyo, Japan; PoS (WPCF2011) 003.

[14] W. N. Zhang, M. J. Efaaf, and C. Y. Wong, Phys. Rev. C **70**, 024903 (2004).

[15] W. N. Zhang, Y. Y. Ren, and C. Y. Wong, Phys. Rev. C **74**, 024908 (2006).

[16] W. N. Zhang, Z. T. Yang, and Y. Y. Ren, Phys. Rev. C **80**, 044908 (2009).

[17] C. Adler *et al.* (STAR Collaboration), Phys. Rev. Lett. **87**, 082301 (2001).

[18] K. Adcox *et al.* (PHENIX Collaboration), Phys. Rev. Lett. **88**, 192302 (2002).

[19] S. S. Adler *et al.* (PHENIX Collaboration), Phys. Rev. Lett. **93**, 152302 (2004).

[20] J. Adams *et al.* (STAR Collaboration), Phys. Rev. C **71**, 044906 (2005).

[21] W. N. Zhang, talk at The Seventh Workshop on Particle Correlations and Femtoscopy, September 20-24, 2011, Tokyo, Japan; PoS (WPCF2011) 051.

[22] W. N. Zhang, H. J. Yin, and Y. Y. Ren, Chin. Phys. Lett **28**, 122501 (2011).

[23] A. Adare, M. Luzum, H. Petersen, Phys. Scripta **87**, 048001 (2013); arXiv:1212.5388[nucl-th]

[24] C. Y. Wong, Ann. Phys. **77**, 279 (1973).

[25] G. Torrieri, B. Tomášik, I. Mishustin, Phys. Rev. C **77**, 034903 (2008).

[26] J. Takahashi, B. M. Tavares, W. L. Qian *et al.* Phys. Rev. Lett. 103, 242301 (2009).

[27] D. J. Bjorken, Phys. Rev. D **27**, 140 (1983).

[28] C. Shen, U. Heinz, P. Huovinen, and H. C. Song, Phys. Rev. C **82**, 054904 (2010).

[29] S. Voloshin and Y. Zhang, Z. Phys. C **70**, 665 (1996).

[30] A. M. Poskanzer and S. A. Voloshin, Phys. Rev. C **58**, 1671 (1998).

[31] S. S. Adler *et al.* (PHENIX Collaboration), Phys. Rev. C **69**, 034909 (2004).

[32] J. Adams *et al.* (STAR Collaboration), Phys. Rev. Lett. **92**, 112301 (2004).

[33] J. Adams *et al.* (STAR Collaboration), Phys. Rev. C **72**, 014904 (2005).

[34] M. Gyulassy, S. K. Kauffmann, and L. W. Wilson, Phys. Rev. C **20**, 2267 (1979).

[35] C. Y. Wong, *Introduction to High-Energy Heavy-Ion Collisions* (World Scientific, Singapore, 1994), Chap. 17.

[36] U. A. Wienemann and U. Heinz, Phys. Rep **319**, 145 (1999).

[37] R. M. Weiner, Phys. Rep **327**, 249 (2000).

[38] M. A. Lisa, S. Pratt, R. Soltz, U. Wiedemann, Annu. Rev. Nucl. Part. Sci **55**, 357 (2005).

[39] G. Bertsch, M. Gong, and M. Tohyama, Phys. Rev. C **37**, 1896 (1988); G. Bertsch, Nucl. Phys. A **498**, 173c (1989).

[40] S. Pratt, T. Csörgo, and J. Zimányi, Phys. Rev.C **42**, 2646 (1990).

[41] J. Yang, Y. Y. Ren and W. N. Zhang, Advances in High Energy Physics, 2014, 846154 (2014).